Andean Geology 53 (1): 80-97. January, 2026
doi: 10.5027/andgeoV53n1-3802

Andean Geology
www.andeangeology.cl

SARIMA-based streamflow forecasting in the San Juan River, Arid Andes

***Cristian Villarroel[1, 2], Monica Morvillo[3], Emmanuel Ocaña[1, 3], María Yanina Esper Angillieri[1], Eduardo Kruse[4, 5]**

[1] *Geosphere and Biosphere Research Centre - National Council for Scientific and Technical Research (CIGEOBIO-CONICET), av. Ignacio de la Roza 590 (Oeste), Rivadavia, San Juan, Argentina.*
Orcid ID: https://orcid.org/0000-0002-1576-0147
cristian.villarroel@unsj-cuim.edu.ar, raulemmanuelo@gmail.com, yaninaesper@gmail.com

[2] *Faculty of Exact and Natural Sciences, National University of Cuyo (FCEN-UNCUYO), Padre Jorge Contreras 1300, Parque General San Martín, Mendoza, Argentina.*

[3] *Faculty of Exact, Physical and Natural Sciences, National University of San Juan (FCEFyN-UNSJ), av. Ignacio de la Roza 590 (Oeste), departamento Rivadavia, San Juan, Argentina.*
mmorvillo@hotmail.com

[4] *Faculty of Natural Sciences and Museum, National University of La Plata (FCNyM-UNLP), Avenida 122 y 60, La Plata, Argentina.*
eduardokruse@gmail.com

[5] *National Council for Scientific and Technical Research (CONICET), calle 8 N° 1467, La Plata, Argentina.*

** Corresponding author: cristian.villarroel@unsj-cuim.edu.ar*

ABSTRACT. River water is a vital resource for human consumption, industrial use, power generation, and recreational activities, among other uses. A number of techniques are currently available to forecast streamflow at different temporal scales, although such approaches usually require different types of input data. The aim of this study is to analyze the long-term hydrological behavior of the San Juan River, located in the Arid Andes of Argentina, a region facing severe water scarcity. A Seasonal Autoregressive Integrated Moving Average (SARIMA) statistical model was applied to project future annual streamflow volume (Hm^3) dynamics up to the 2070-2071 hydrological cycle. The results indicate a general downward trend. Over the next decade, critical low-flow periods are expected, similar to those observed in recent years. For the 2026-2029 period, projected flows are slightly above the average total annual consumption level (1,200 Hm^3), yet insufficient to fully restore ecosystems affected by previous prolonged droughts. In contrast, for the 2030-2035 period, forecasts suggest a sharp decline in streamflow to around 680 Hm^3, nearly half the current annual consumption. These findings provide a solid basis for developing adaptive strategies to manage potential future water availability scenarios effectively.

Keywords: Arid Andes, Streamflow forecast, Drought, Statistical model.

RESUMEN. Pronóstico de caudal en el río San Juan, Andes áridos, basado en el modelo SARIMA. El agua de los ríos constituye un recurso vital para el consumo humano, el uso industrial, la generación de electricidad y las actividades recreativas, entre otros fines. En la actualidad, existen diversas técnicas para predecir el caudal de un río en diferentes escalas temporales; sin embargo, dichas metodologías usualmente requieren distintos tipos de datos de entrada para alimentar sus modelos predictivos. El objetivo de este estudio es analizar el comportamiento hidrológico de largo plazo del río San Juan, ubicado en los Andes áridos de Argentina, una región caracterizada por una marcada escasez hídrica. Para ello, se aplicó un modelo estadístico Autorregresivo Integrado de Media Móvil Estacional (SARIMA, por sus siglas en inglés), con el fin de proyectar la evolución futura del escurrimiento anual (Hm^3) hasta el ciclo hidrológico 2070-2071. Los resultados obtenidos muestran, en general, una tendencia descendente para este parámetro. En la próxima década, se prevén períodos críticos de bajos volúmenes de agua, comparables a los registrados en eventos recientes. Para el período 2026-2029, se estiman valores levemente superiores al promedio de consumo anual total (1.200 Hm^3), aunque insuficientes para la recuperación integral de los ecosistemas afectados por las prolongadas y severas sequías precedentes. En cambio, para el período 2030-2035, las proyecciones indican una caída abrupta del escurrimiento anual hasta aproximadamente 680 Hm^3, cifra que representa casi la mitad del consumo anual actual. Estos resultados ofrecen una base sólida para el diseño de estrategias de adaptación y gestión sostenible frente a los distintos escenarios futuros de disponibilidad hídrica.

Palabras clave: Andes áridos, Pronóstico de caudal, Sequía, Modelo estadístico.

1. Introduction

Water, both surface and groundwater, is the most important substance for life and ecosystem development. Due to its nature and needs, mankind has confined the construction of settlements to sites with water availability of good quality.

In arid regions, water is predominantly stored and drained from the ground and/or subsurface to a greater extent than from the surface. This is because water bodies in contact with the atmosphere tend to undergo evaporation processes due to high temperatures, low precipitation, and lack of air humidity (Scanlon *et al.*, 2005). When available and of sufficient quantity and quality, surface water is often preferred as the main source of supply due to the ease in collection and management, with groundwater playing a greater role at times of surface water scarcity (Siebert *et al.,* 2010).

Surface water is a key indicator of changes in basin hydrological balances, influenced by alterations in water uses or to environmental shifts associated with meteorological or climatic conditions (Babel *et al.*, 2020; Ríos *et al.*, 2025). Streamflow forecasting is inherently challenging due to the complexity of the hydrological system itself and its non-linear behavior (Wang *et al.*, 2006; Zhang *et al.*, 2018). Several approaches have been developed over the last few decades to enhance the accuracy of these forecasts, being a recent one that combines hydrological and statistical models with Artificial Intelligence (AI) tools (Núñez *et al.*, 2023). However, the choice of which model to use depends on multiple factors, including basin characteristics, desired forecast period, data availability and frequency, and methods for measuring uncertainty, among other considerations.

In recent studies, AI has been increasingly applied to solve a wide range of problems in hydrology and water resources management (Biazar *et al.*, 2025). Among these applications, time series forecasting models such as SARIMA (S: Seasonal, AR: Autoregressive, I: Integrated, MA: Moving Average) have been enhanced through AI-based modules to improve predictive accuracy in hydrological systems. Nowadays, the emergence of Explainable Artificial Intelligence (XAI) is offering a promising pathway to address the long-standing trade-off between prediction performance and interpretability in AI-driven hydrological modeling. However, despite these important advances, and with the exception of Australia, countries in the Southern Hemisphere have made limited contributions to the development and application of XAI in this domain, being the Núñez *et al.* (2023) study one of such exceptions.

Certain authors have limited the benefits of the ARIMA-SARIMA models for predicting non-linear hydrological processes, claiming that AI tools (*e.g.*, Artificial Neural Network, Support Vector Machine) work better under certain hydrological conditions (Wu *et al.*, 2014; Zhang *et al.*, 2018; Thakur *et al.*, 2020). However, the predictive capacity of such numerical approaches is reduced to relatively short forecasting horizons because it does not incorporate parameters to describe the general characteristics of runoff fluctuations (cf. Zhang *et al.*, 2018). Statistical modeling, on the contrary, has no time limits for prediction and has the advantage of associating probabilistic intervals that allow covering the occurrence of extreme values throughout the prediction period. Linearity and normality do not limit the use of statistical models, as deviations from these assumptions can be addressed through variable transformations and subsequent back-transformation of the predictions.

The San Juan River is the sole surface water source available for a population of approximately 0.8 million inhabitants. To the best of the authors' knowledge, there is only one short-term prediction model for the San Juan River streamflow (Dolling and Varas, 2002). The present contribution, on the contrary, aims to analyze the historical trends of the San Juan River streamflow, examine its intra- and inter-annual behavior patterns (cyclicity and/or periodicity), and establish short- and long-term prediction mechanisms, building a streamflow forecast model. Here, we used the SARIMA model, which has successfully been used for streamflow forecasting elsewhere (Valipour, 2015; Zhang *et al.*, 2015).

At present, the San Juan Province is experiencing one of the longest and most severe droughts (2010-present) on record (Garreaud *et al.*, 2017; Rivera *et al.*, 2017, 2021). The San Juan River's 2021-2022 annual runoff (536 Hm^3) has been the lowest so far in the historical record (1909-2023). Moreover, water stored in the dams acting as reservoirs (Ullum, Punta Negra, and Caracoles) sums only ~217 Hm^3, which is just 14% of the maximum storable volume. On average, the province requires around 1,200 Hm^3 annually for human consumption, irrigation and industrial activity. These numbers illustrate the severity of the ongoing water crisis in

this region. Its effects are already impacting various productive sectors, as water allocations for irrigation have temporarily been cut off to prioritize water for human consumption (https://hidraulica.sanjuan.gob.ar/). During the 2022-2023 period, the cut off was in place for ~one third of the year.

SARIMA-based streamflow forecasts are valuable tools for identifying potential future scenarios that can support informed land management decisions, ultimately reducing vulnerability to catastrophic events such as the severe droughts currently affecting the region.

2. Study area

The hydrological behavior of the San Juan River is highly variable both on a seasonal and year-to-year basis, with an average annual streamflow and runoff for the 1909-2021 period of 60.9 m^3/s and 1,955 Hm^3, respectively (https://hidraulica.sanjuan.gob.ar/). The river is nival in origin, *i.e.*, its streamflow can be explained by the summer snowmelt accumulated during the previous winter (Bruniard and Moro, 1994; Poblete and Hryciw, 2017), with its behavior depending mainly on cryogenic conditions in the headwaters of the basin (Massone *et al.,* 2016; Rodríguez *et al.*, 2016; Crespo *et al.*, 2017; Arenson *et al.*, 2022) and to a much lesser extent on contributions from transient summer storms (Vich *et al.*, 2016). Winter snowpacks and summer streamflows are, in general, highly correlated, although this relationship becomes less significant during drought periods (Masiokas *et al.*, 2006). Glacial and periglacial processes dominate the cold, high-altitude, headwaters of the basin (Villarroel *et al.*, 2018; Tapia-Baldis, 2019; Tapia-Baldis and Trombotto-Liaudat, 2020).

The region's climate system is controlled primarily by its subtropical latitudinal location, which is influenced by the Pacific subtropical anticyclone and phenomena like ENSO (El Niño Southern Oscillation), and its leeward position in the Andes (Minetti *et al.*, 2007; Garreaud, 2009; Viale and Norte, 2009; Poblete and Castro, 2021). Furthermore, the San Juan Province belongs to the bioclimatic region of the South American Arid Diagonal (Bruniard, 1982; Abraham *et al.*, 2020). As a result, it has a characteristic water deficit caused by a high potential evapotranspiration that far exceeds its low rainfall (Poblete and Minetti, 1989). This scarcity of surface water resources has been intensifying over time (Rivera *et al.*, 2021).

The Andean sector has a cold and arid climate, with its precipitation almost exclusively in the form of snow (Gascoin *et al.*, 2011). Annual precipitation varies dramatically during the cooling and warming phases of ENSO, with 60-70 and >1100-1200 mm, respectively (Montecinos and Aceituno, 2003; Zech *et al.*, 2017). Solar radiation is very intense, averaging 400 W/m^2 per year for the 4,100-4,700 m a.s.l. altitude range (Schrott, 1991). As for the mean annual temperature, the 0 °C isotherm in the Arid Andes decreases in elevation from north to south, transitioning from approximately 4,300 to 3,700 m a.s.l. (Tapia-Baldis *et al.*, 2019). The lowest areas are located east of the San Juan River basin, at an average elevation of 800 m a.s.l., where a mean annual temperature of 16.7 °C, and <100 mm of annual rainfall, mostly in the form of torrential rains during the summer months, are prevalent (Müller and Lovino, 2023).

In terms of monitoring, a gauging station is located in the San Juan River at the km 101 mark in the National Route 149 (Fig. 1). Other stations are the Álvarez Condarco in the Blanco River and the La Plateada station in the Los Patos River, where average annual streamflows of 24.4 and 49.9 m^3/s have been measured, respectively.

3. Methodology

3.1. Data source and collection

Streamflow data from the km 101 gauging station were used for this study. As this station is located in the middle sector of the basin, the streamflows measured there are not affected by the dams built downstream. The data were extracted from the https://hidraulica.sanjuan.gob.ar/ website for the 1909-2021 period. For the purpose of this case study application, the data were transformed from average monthly streamflow (m^3/s) into semi-annual runoff (Hm^3) values for the cold (April-September) and warm (October-March) periods. The warm period corresponds to snow and ice melting, while the cold period represents snow and ice accumulation. Thus, a total of 224 semi-annual runoff values were obtained. The semi-annual runoff data were used to build the predictive model, whose results were shown on an annual scale, after combining two consecutive semi-annual periods.

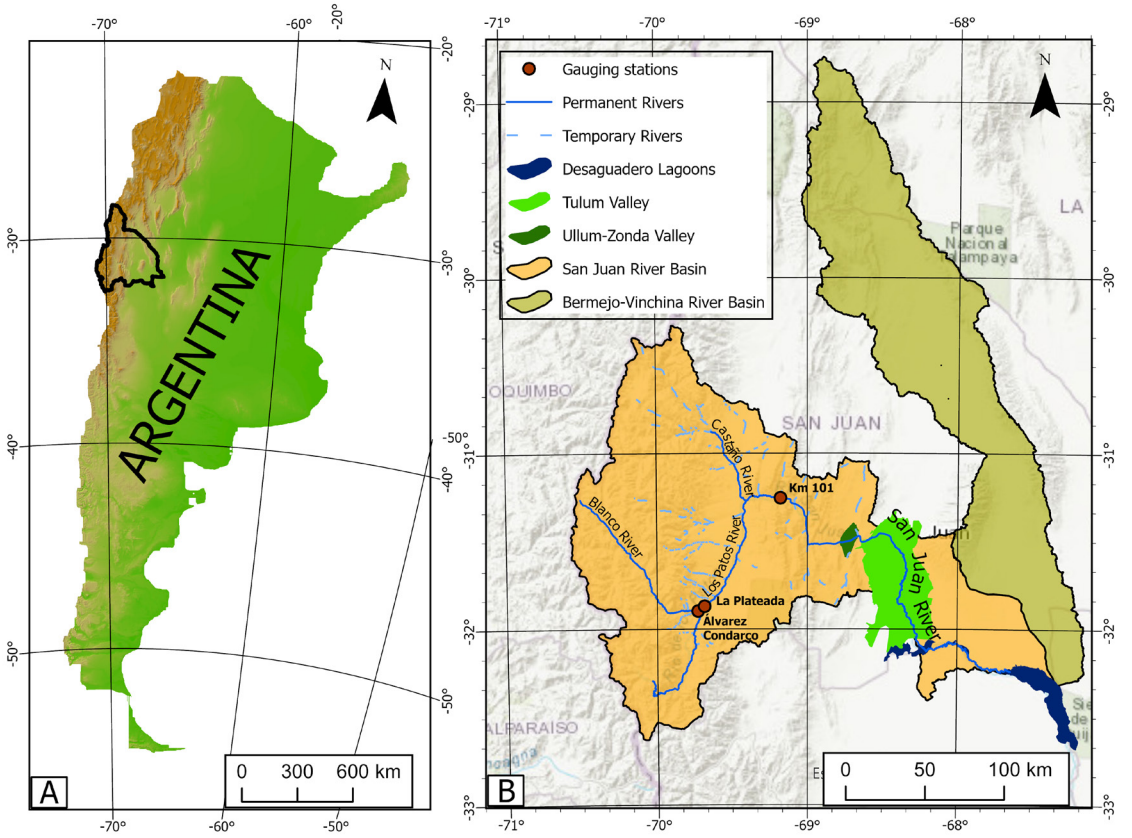

FIG. 1. **A**. Location map of the San Juan Province in Argentina. **B.** Main rivers, valleys, and river basins. The gauging stations mentioned in the text are shown as well.

The SARIMA model presented here was developed using the R package *forecast* (Hyndman and Khandakar, 2008; Costa *et al.*, 2023; Larance *et al.*, 2025).

3.2. Models for stochastic processes

A time series Y_t ($t = 1 \ldots T$) is considered a realization of a stochastic process that can be described and predicted using parametric models such as the SARIMA model (Box and Jenkins, 1970). Basically, these models represent a current series value with information contained in previous data (autoregressive part, parameter p) and random errors (moving average part, parameter q). The statistical stationarity (constant mean) requirement is relaxed by including a third parameter d: integration or differentiation.

The most comprehensive, flexible and parsimonious approach to represent a stochastic process is the multiplicative SARIMA (p,d,q)(P,D,Q)[s] model. With a limited set of parameters, it is possible to determine regular trends, seasonalities or cycles occurring every s time units, as well as the potential interactions between the two components (Ioannidis and Nikolakakou, 2025). Its compact notation is:

$$\phi_p(L)\Phi_P(L^s)\Delta^d\,\Delta_s^D\,Y_t = \theta_q(L)\Theta_Q(L^s)a_t$$

Where L is the lag (or backshift) operator, which operates on an element of the time series to produce theprevious element, $\phi_p(L)$ and $\theta_q(L)$ denote respectively the autoregressive and moving average polynomials for the regular part (d being the order of integration for the regular part). $\Phi_P(L^s)$ and $\Theta_Q(L^s)$ refer respectively to the autoregressive and moving average polynomials for the seasonal part (D being the order of integration for cyclicity). a_t is the white noise error term $\sim WN(0, \sigma^2)$, which specifies $E(a_t)=0, Var(a_t)=\sigma^2$, and $cov[a_t, a_{t-j}] = 0$ for $j \neq t$.

Such an approach is equivalent to describing the data as the sum of a deterministic component (expectation) and a stochastic component (white noise). Under the assumption of normal distribution, the parameters are estimated by maximum likelihood and then used to predict a new piece of data.

3.3. SARIMA model construction

The methodology to construct the appropriate SARIMA (p,d,q)(P,D,Q)[s] model for a seasonal time series Y_t comprises the identification, estimation and validation, and prediction phases (Kabbilawsh *et al.*, 2022; Muthee *et al*., 2023). These phases are explained below.

3.3.1. Identification

This phase is intended to propose the model (or models) that can represent the evolution of the Y_t series. First, the stationarity in the variance is analyzed through graphs. Any lack of stationarity is resolved by applying variance-stabilizing transformations. A generic transformation resource in SARIMA-case applications is the Box-Cox method or the logarithm over range translations (X±C) when positive asymmetries are present. Series graphs, autocorrelation function (ACF) and partial autocorrelation function (PACF) graphs, and unit root contrasts are then examined to determine the stationarity of the mean and note the presence of both regular trends corrected with the parameter d and seasonal behavior corrected with D and s. This leads to a SARIMA (p,d,q)(P,D,Q)[s] model proposal.

Parameter identification is a time-consuming process as it requires repeated tests until the estimation and validation results are adequate; it may even lead to rethinking the complexity of the model.

3.3.2. Estimation and validation

Once the parameter order is set, an estimation is performed by maximum likelihood under the assumption of normality, obtaining the fit measure (log likelihood) and each polynomial's coefficients together with their standard errors. Measurement of predictive errors for a training data set is also considered for model diagnosis and validation: Mean Error (ME), Mean Squared Error (MSE), Root Mean Squared Error (RMSE), Mean Absolute Error (MAE), Mean Percentage Error (MPE), Mean Absolute Percentage Error (MAPE), Mean Absolute Scaled Error (MASE), and Autocorrelation of Errors at Lag 1 (ACF1). All these errors must verify the white noise hypothesis, both graphically and analytically (Ljung-Box test), show no correlation structure and, where possible, adjust to a normal model (Jarque-Bera test).

3.3.3. Prediction

Here, the goal is to obtain the best predictor $Y_T(l)$ for a future value Y_{T+l}, where T denotes the last observed instant and l the number of periods in the future. This is achieved by minimizing the mean squared of prediction error $e_T(l) = E[Y_{T+l} - \hat{Y}_T(l)]^2$, which is equivalent to determining the conditional expectation to the data set I_T:

$$\hat{Y}_T(l) = E[Y_{T+l} \mid I_T]$$

The optimal prediction, under the assumption of normality for the white noise error term, allows associating a probability interval to a specific prediction $\hat{Y}_T(l)$. Specifically, the prediction error is normally distributed with zero mean and variance $V(e_T(l))$, that is:

$$e_T(l) \sim N(0, V(e_T(l)))$$

which enables the construction of a $(1-\alpha)$ prediction interval around the forecasted value. This interval provides a probabilistic measure of the uncertainty associated with the prediction and represents a range within which the future realization is expected to lie with probability $1-\alpha$, *i.e.*:

$$P\left[\hat{Y}_T(l) - N_{1-\frac{\alpha}{2}}\sqrt{V(e_T(l))} < Y_T(l) < \hat{Y}_T(l) + N_{1-\frac{\alpha}{2}}\sqrt{V(e_T(l))}\right] = 1-\alpha$$

4. Results

4.1. SARIMA model

Figure 2A shows the histograms for the original series Y_T and the transformed series $Z_t = ln(Y_t - 266)$, for which the asymmetry coefficient is -0,0024. The symmetry of the transformed series favors compliance with the optimal normality condition of the model. This, in turn, makes it possible to complement the prediction with probability intervals. The Y_t series exhibits non-stationary behavior in its variance,while the Z_t series stabilizes the variance and enables residuals to be normalized (Fig. 2B).

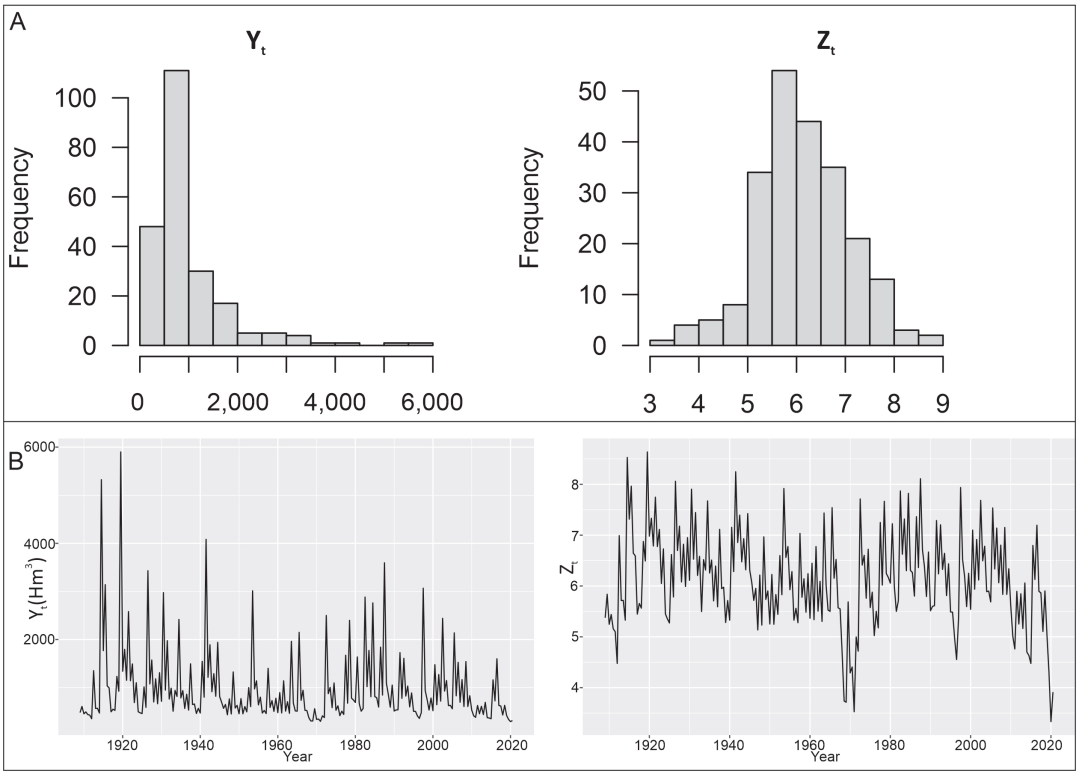

FIG. 2. Histograms (**A**) and time series (**B**) for the original variable Y_T and the transformed variable Z_t. Panel A shows that the transformation reduces skewness and improves symmetry, favoring compliance with the normality assumption required by the SARIMA model. Panel B illustrates how the transformation stabilizes the variance of the series through time, a necessary condition for subsequent stationarity analysis and model fitting.

As figure 3 shows, although the transformed series has a stable variance, it is not stationary at the mean, fluctuating around a straight line whose negative slope, although gentle, is statistically significant, as indicated by a p-value of 0.0062.

The Z_t series has varied behavioral cycles. In fact, according to the successive peaks and depressions (Fig. 3) and the comparative synthesis represented in boxplot format (Fig. 4), seasonality is observed in a 2-semester cycle between the warm and cold averages. By extending the time scale, a pattern of minimum values is detected in periods ranging from 10 to 14 semesters (green segmented lines of figure 3). The time series also reveals minimum values occurring at distinct temporal scales. Specifically, intermediate-period minima are observed at intervals ranging from 47 to 62 semesters (blue segmented lines in figure 3), whereas longer-term and more extreme minima occur at intervals between 100 and 116 semesters (black segmented lines in figure 3).

The non-stationarity in the mean, such as the presence of a seasonal structure (P,D,Q)[s], is confirmed from the non-zero ACF function coefficients and the oscillations with peaks and plateaus extending up to lag 126 (Fig. 5).

4.2. Time series modelling

The (0,0,1)(1,1,1)[2] model parameters were identified from the *auto.arima* function of the R project's forecast library (model fit and validation measures shown in table 1; log likelihood = -206.58). However, since seasonal patterns and extreme peaks contrary to the white noise hypothesis remained, the residual plot obtained with the automatic estimation method was deemed not satisfactory (Fig. 6).

New (p,d,q)(P,D,Q)[s] values were therefore tested taking into account the significant ACF correlations indicating recurrent long-term cycles (Fig. 5). Some of the tests conducted are shown in table 2, of which

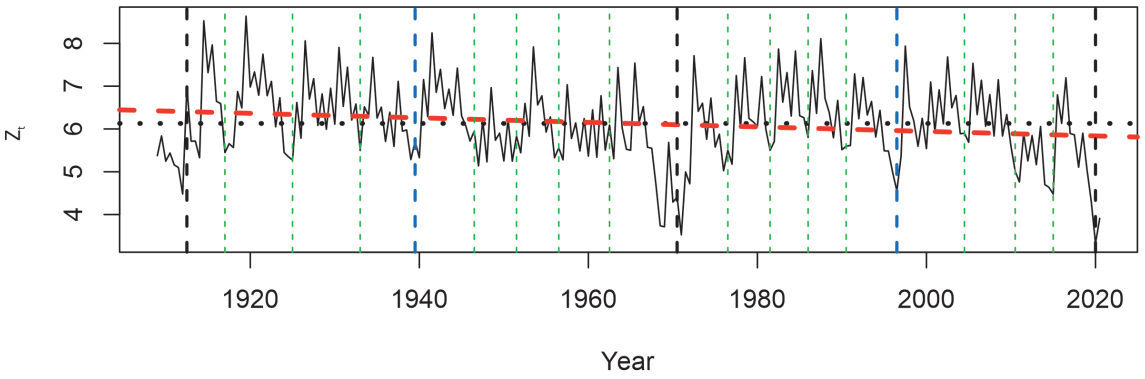

FIG. 3. Trend and cyclicity for the transformed time series Z_t (as shown in figure 2B). The red segmented line represents the linear trend $16.5 - 0.0053 \times t$, where t is the time in years. The horizontal dotted black line indicates the long-term mean value of the transformed series for the entire study period. Vertical, segmented lines highlight minimum values occurring at different temporal scales: green lines indicate short-term minima (10-14 semesters), blue lines represent intermediate recurrence intervals (47-62 semesters), and black lines denote long-term and extreme minima (100-116 semesters).

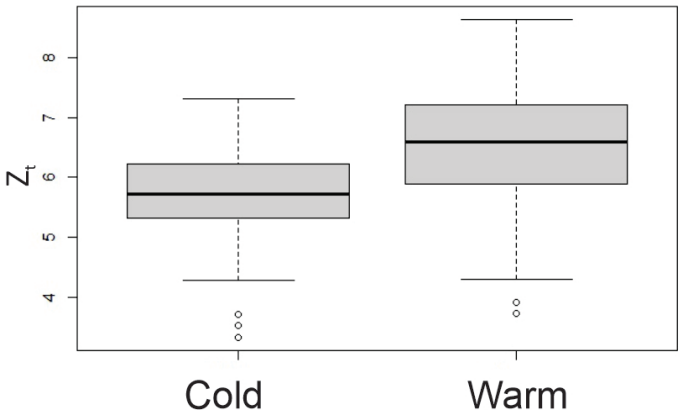

FIG. 4. Boxplot showing the seasonality of the transformed time series Z_t. Circles denote outliers. The figure highlights greater dispersion during the warm semester, suggesting increased streamflow variability.

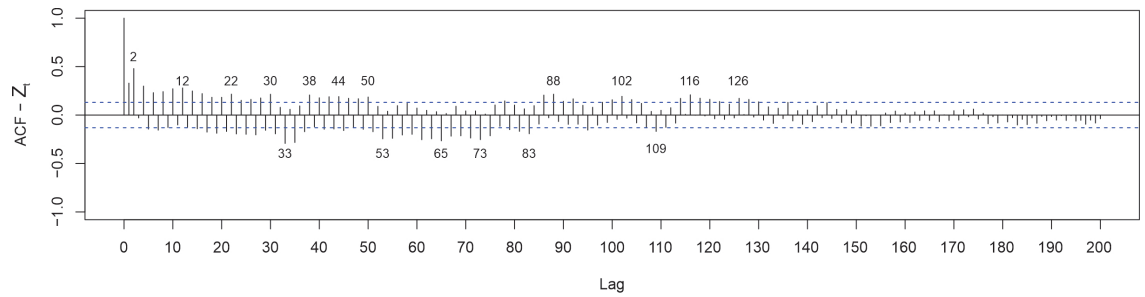

FIG. 5. Autocorrelation function (ACF) plot for the transformed variable Z_t. The plot displays the correlation of the series with its own lagged values. The dashed blue lines represent the 95% confidence interval. Significant peaks out of these bounds indicate temporal dependencies or recurring patterns.

TABLE 1. ESTIMATED COEFFICIENTS IN THE (0,0,1)(1,1,1)[2] SARIMA MODEL.

ME	RMSE	MAE	MPE	MAPE	MASE	ACF1
-0.019719	0.602200	0.434701	-1.216997	7.285422	0.605157	-0.016462

ME: Mean Error. **RMSE**: Root Mean Squared Error. **MAE**: Mean Absolute Error. **MPE**: Mean Percentage Error. **MAPE**: Mean Absolute Percentage Error. **MASE**: Mean Absolute Scaled Error (MASE). **ACF1**: Autocorrelation of Errors at Lag 1.

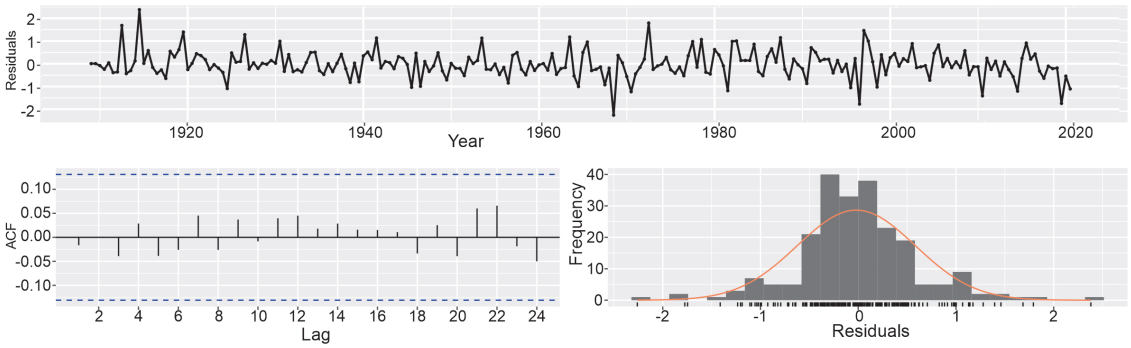

FIG. 6. Model residuals' analysis (0,0,1)(1,1,1)[2]. The top panel shows standardized residuals over time, with no apparent structure. The ACF plot (bottom left) confirms the absence of significant autocorrelations (95% confidence interval represented by dashed blue lines). The histogram (bottom right) suggests approximate normality, supporting the white noise assumption.

TABLE 2. FIT, PREDICTION AND VALIDATION MEASURES FOR DIFFERENT SARIMA MODELS TESTED. LAST COLUMN (IN GREY), THE MODEL FOLLOWED IN THIS STUDY.

Model Parameters	(p,d,q)	(0,0,1)	(0,0,1)	(1,0,0)	(1,0,0)	(1,0,0)	**(1,0,0)**
	(P,D,Q)[s]	(1,1,1)[2]	(1,1,0)[58]	(1,1,0)[58]	(0,1,0)[106]	(0,1,0) [116]	**(0,1,0)[126]**
Fit measure	log likelihood	-206.580	-188.500	-185.450	-145.230	-126.880	-115.650
Training set error measures	ME	-0.020	-0.103	-0.059	-0.050	-0.061	-0.043
	RMSE	0.602	0.599	0.596	0.600	0.543	0.520
	MAE	0.435	0.382	0.366	0.313	0.273	0.249
	MPE	-1.217	-2.523	-1.653	-1.450	-1.570	-1.182
	MAPE	7.285	6.656	6.208	5.430	4.755	4.162
	MASE	0.605	0.425	0.408	0.349	0.304	0.277
	ACF1	-0.016	0.180	0.117	0.064	0.127	0.060
p-value	Ljung-Box	0.776	0.000	0.002	0.146	0.003	0.149
	Jarque-Bera	<0.001	$<2.2\times10^{-16}$	0.002	<0.001	0.002	0.087

Key for the training set error measures as in table 1.

the (1,0,0)(0,1,0)[126] model was found to be the best-performing. The seasonal parameter (126) corresponds to differencing between semiannual observations separated by 63 years, which reduces the effective length of the time series and restricts model calibration and forecasting to data from 1972 onward. Its summarized form is as follows:

$$\phi_p(L)\,\Delta_s^D ln(Y_t - 266) = a_t$$

The transformed series graph $(1-L^{126})ln(D-266)$ indicates a non-seasonal but non-stationary behavior (decreasing trend), which is confirmed in the ACF plot and justifies the differentiation $D=1$ (Fig. 7).

The Dickey-Fuller test with stationarity alternative hypothesis confirms, with a p-value of <<0.01, that the series $\Delta_{126}^1 Z_t$ is stationary (Fig. 8).

The (1,0,0)(0,1,0)[126] model estimation process results in $\phi_1 = 0.6096$ with an standard error of 0.0860 (which under normality assumptions corresponds to an approximate 68% confidence interval). The resulting model is specified by:

$$(1 - 0.6096L)(1 - L)(1 - L^{126})ln(Y_t - 266) = a_t$$

Lastly, a 50-year prediction for the series $Z_t = ln(Y_t - 266)$ is shown in figure 9 for the period 2021-2071 (dark blue line), in addition to 80% (pale blue) and 95% (light blue) probability intervals. The complete streamflow forecast results are provided in Supplementary Table 1.

5. Discussion

5.1. Runoff forecasting accuracy

In this section, the ability of the SARIMA (1,0,0)(0,1,0)[126] model to forecast streamflows is analyzed. As mentioned in section 4.2, this model was selected due to its superior performance across various fit measures (Table 2) compared to a wide range of constructed models. Therefore, it stands as the most effective SARIMA model for forecasting streamflows of the San Juan River using the available historical dataset. Model accuracy is calculated as follows:

$$RE = 100 \times (R_o - R_f)/R_o$$

Where RE is the relative error in percentage form, R_o is the observed runoff (Hm^3), and R_f is the

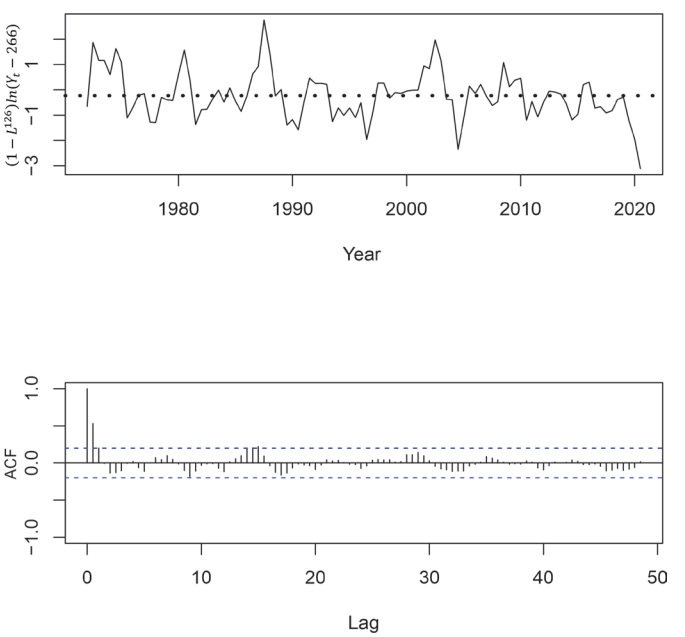

FIG. 7. Transformed time series $\Delta_{126}^1 Z_t = (1 - L^{126})ln(Y_t - 266)$ and its autocorrelation function (ACF). The differentiated series shows stationarity, with the ACF confirming the absence of significant autocorrelations. The horizontal dotted black line in the upper panel indicates the long-term mean value of the transformed series, while the dashed blue lines in the lower panel encompass the 95% confidence interval.

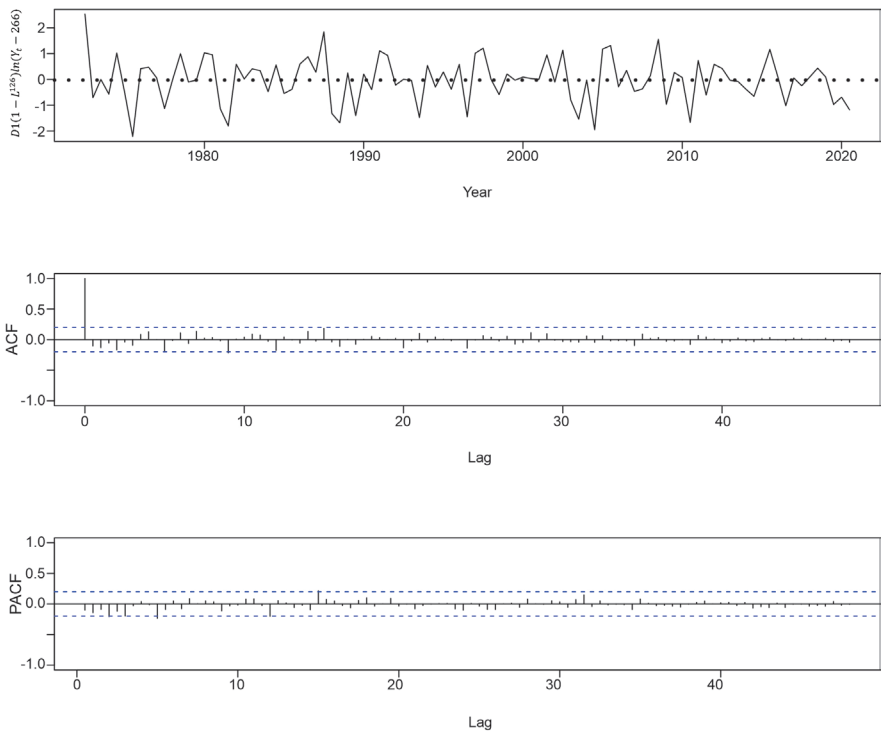

FIG. 8. Graph for the series $\Delta^1_{126} Z_t = D1\,(1-L^{126})ln(Y_t-266)$ and their ACF and PACF correlograms. The results suggest that the series is stationary with weak autocorrelation structure. The horizontal dotted black line in the upper panel indicates the long-term mean value of the transformed series, while the dashed blue lines in the rest of the panels encompass the 95% confidence intervals.

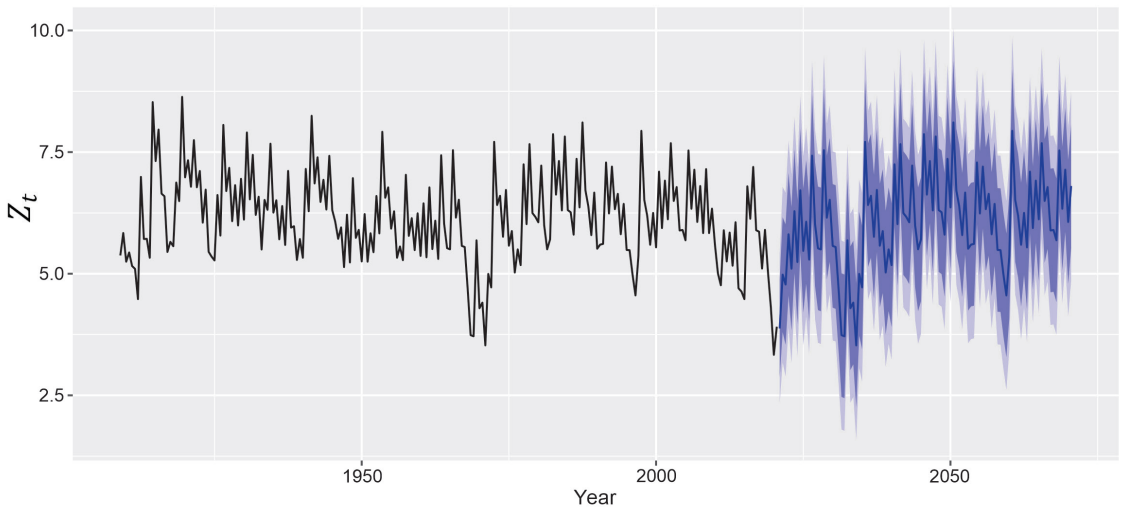

FIG. 9. Fifty-year forecast for the series $Z_t = ln(Y_t - 266)$(dark blue line), including 80% (pale blue area) and 95% (light blue area) confidence intervals.

forecasted runoff (Hm^3). Relative errors are shown in table 3; 54% of the data exhibit acceptable forecasts (classified as excellent, very good, or good), 16% have moderate forecasts, and the remaining 30% are categorized as poor. Additionally, 54% of the data were predicted with a deficit, whereas 46% were forecasted with an excess. When examining the excess or deficit in the predicted values, it can be noted that among the 54% of data with acceptable forecasts, these values (whether excess or deficit) are relatively balanced. Nevertheless, the other categories exhibit different patterns. For instance, in the moderate forecast category, 87.5% of the data were estimated with a deficit, whereas in the poor forecast category, the maximum deficit observed was 58%. Conversely, for values calculated with an excess, the discrepancies are even greater, reaching 780%. This latter group of data includes predicted values that significantly exceed the actual, observed values by several orders of magnitude and are deemed unrealistic from a hydrological perspective (Supplementary Table 2).

The significant discrepancy between the predicted and actual values may be attributed to the reliability of the original data. In the semi-annual runoff data series, two initial (up to year 1920) observations reach maximum values of 5,323 and 5,899 Hm^3 (Fig. 10A). Beyond this point, within the remaining dataset of 202 observations (spanning 101 years), these maximum values are not recorded again; in fact, the closest value is 31% lower than the highest pre-1920 recorded value (Fig. 10A). It is possible that these two unusually high peak values represent overestimations due to the measurement techniques employed at that time. These anomalous maximum values could exert an influence on the SARIMA model. In the validation dataset, there are also two predicted maximum values exhibiting a similar structure to those in the original series (Fig. 10B).

TABLE 3. ACCURACY OF FORECASTED RUNOFF VALUES.

Relative Error (RE)	Data	%
RE < 5 (excellent)	16	16.3
5 ≥ RE < 10 (very good)	16	16.3
10 ≥ RE < 20 (good)	21	21.5
20 ≥ RE < 30 (moderate)	16	16.3
RE ≥ 30 (poor)	29	29.6
Total	98	100

5.2. Decomposing the time series

The additive decomposition of a time series allows for the identification of the components that must be represented in the model. This includes determining whether the series has a constant mean, exhibits pure seasonality, or, in more complex cases, displays multiple seasonalities, trends, and potential interactions between these components, in addition to defining the structure or complexity of the model (Ghide *et al.*, 2022). In our case study, the first component, referred to as the trend, is represented by a moving average that indicates the series does not have a constant mean and displays multiple cyclical patterns. The seasonal component reflects variations around the trend within the smallest periodic unit (2). Finally, the remainder component (irregular or unstructured) is determined by the difference between the observed data and the two preceding components (Fig. 11).

In the second and third phases of parameter estimation and validation (Section 3.3.2), the optimal model was determined based on the AIC (Akaike Information Criterion), RMSE, MAPE, and p-value from the Ljung-Box test. The value of 126 defined a new series of 98 data points through differentiation, revealing a trend function that does not exhibit a constant mean but instead shows cycles of varying lengths that can be attributed to different causes or factors. Identifying the various hydro-climatological factors and their impact on the flow of the San Juan River is, however, beyond the scope of this study. Future research should delve into these aspects in greater detail to gain a better understanding of the hydrological dynamics at play.

5.3. Hydrological status and streamflow forecasting

Streamflow forecasting under the SARIMA model (Fig. 9) does not suggest adequate recovery for the average annual consumption (1,200 Hm^3) over the next 10 hydrological cycles (from 2025-2026 to 2034-2035) (Supplementary Table 1). Measured runoff for the recent cycles 2021-2022, 2022-2023, and 2023-2024, were recorded at 536, 1,010 and 1,061 Hm^3, respectively. These are insufficient to restore the approximately

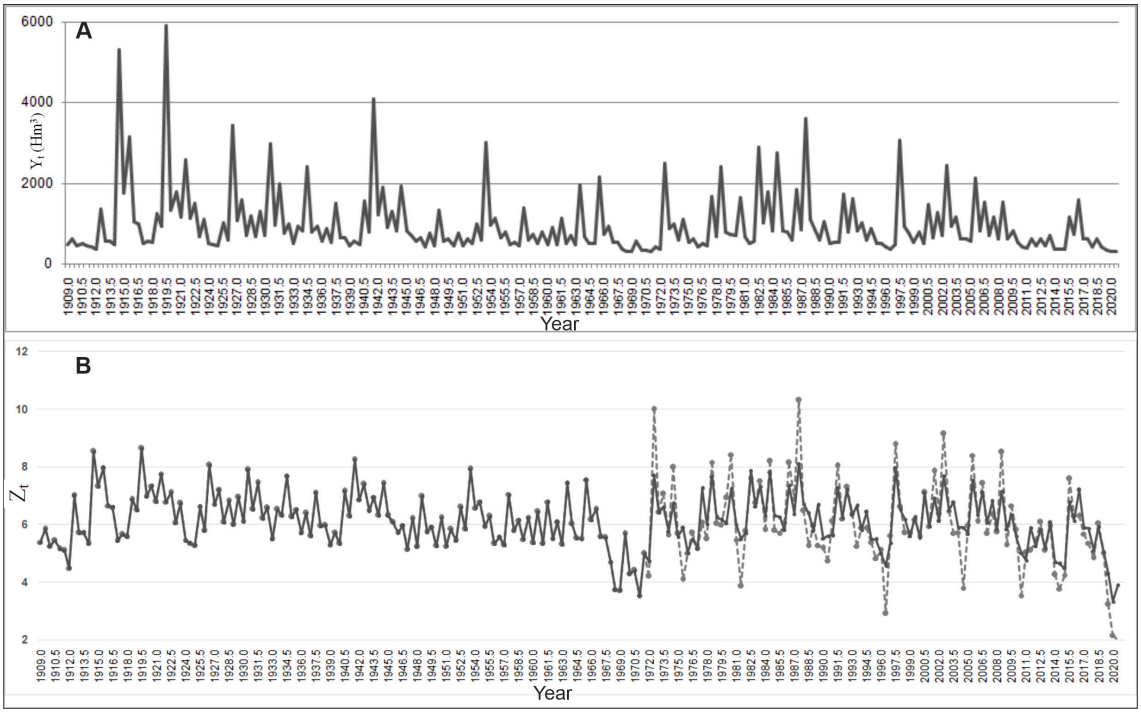

FIG.10. **A.** Original variable Y_t of semi-annual runoff (Hm^3). Two highly anomalous (>5,300 Hm^3) data points are observed at the beginning of the series (1914 and 1919). **B.** Transformed variable Z_t of semi-annual runoff. The solid gray line indicates the observed data, while the segmented gray line represents the forecasted data.

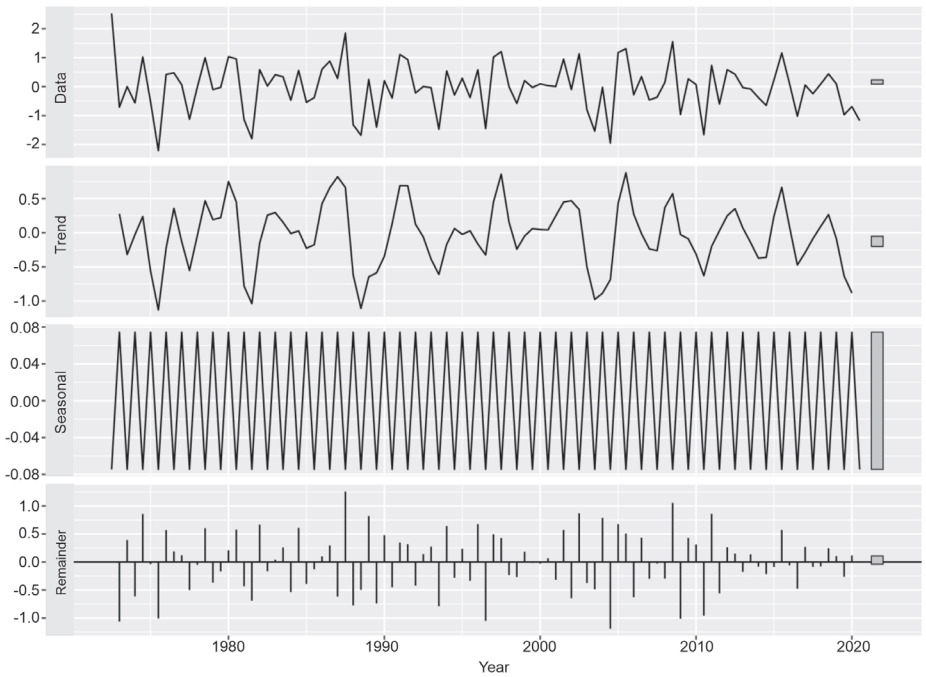

FIG. 11. Decomposing time series showing the trend, seasonal and remainder components. Uppermost panel shows the data series (as depicted in figure 8). Grey bars on the right of each panel represent scale references for each component.

700 Hm^3 values observed during the two previous cycles (2019-2020 and 2020-2021) (Supplementary Table 2). Compounding this issue are the critically low water reserves in dams and the desiccation of wetlands, which create an alarming hydrological situation. In the medium term, the reserves in dams would increase slightly over the next 10 cycles given the annual forecasted fluctuations with respect to average consumption. This is because the positive surpluses predicted for the period 2025-2029 would decrease due to a new deficit in the 2030-2035 period (Supplementary Table 1). This means that even the most abundant cycles under the current drought conditions may not be sufficient to recover higher reservoir storage levels in the dams. The significant, albeit slight, negative trend of decreasing average annual runoff revealed over the 112-year observation period (segmented red line in figure 3), is consistent with the lack of stationarity in cycles longer than 60 years corrected in the SARIMA model by the differencing/integration parameter ($D = 1$). The changes in general large-scale atmospheric circulation patterns and the southward expansion of the Hadley circulation cell have also been observed by others, arguing for a continuously decreasing precipitation trend, and consequently in runoff (Poblete and Minetti, 2017; Cook *et al.*, 2020; Fahad *et al.*, 2020; Rivera *et al.*, 2021).

The only previous study applying Artificial Neural Network in the San Juan River basin utilized a hydro-climatological data series of 17 years (Dolling and Varas, 2002). While this approach may be correct from a numerical perspective, it falls short as a statistical method. Furthermore, in hydrological-climatological studies it is advisable to have data records spanning 30 years or more to cover climatic variability (Devasthale *et al.*, 2023). Hydro-climatological data series for this region of the Andes are not extensive enough to allow streamflow forecasting based on artificial intelligence techniques.

Recently, in the Tupungato River basin, located ~210 km south of the San Juan River, the Support Vector Regression (SVR) technique was applied for the first time to forecast short-term (1 month) flows (Korsic *et al.*, 2023). In that study, SVR results were compared with those from the Classification and Regression Tree (CART) and the ARIMA model, concluding that SVR outperformed the other two methods. Besides this, an additional advantage of the SVR approach is that it uses easily accessible variables (*e.g.*, precipitation, air temperature, streamflow, snow-related indices), solving the lack of data in these remote regions. A limitation of the Korsic *et al.* (2023) study is that the series of hydro-climatological data is only 17 years in length.

While the SVR model mentioned above demonstrated good streamflow prediction results in the short-term, there remains a gap in addressing long-term (>years) forecasting. Long-term approaches, such as the one undertaken here, are essential for developing adaptation strategies to different hydrological scenarios. To the best of the authors' knowledge, no long-term flow forecasts have been conducted for the San Juan River basin to date.

The ARIMA model used in the work of Korsic *et al.* (2023) was selected using the *auto.arima* function in R. Nevertheless, just as discussed in the SARIMA model section, the model that best fits is generally obtained from testing various parameters considering the significant correlations of the ACF function. This suggests that an alternative ARIMA model may yield better performance than the one used in the Korsic *et al.* (2023). Moreover, the training set comprised only 10 years of data, which is insufficient to adequately cover the potential variability of the streamflows.

In the Arid Andes, previous studies that have conducted streamflow forecasts with machine learning or other techniques are insufficient to ascertain which demonstrate superior performance. On the one hand, data availability is very scarce; on the other, forecasts are predominantly focused on short-term predictions. Our case study benefits from an extensive 112-year period data set, which enables a detailed analysis of trends and fluctuations that may be cyclical, periodic or seasonal in nature. These tendencies are parameterized within the statistical modeling framework in a SARIMA environment. Therefore, a SARIMA model can be a valuable technique for predicting flow behavior in this region.

Finally, although the 112-year streamflow record for the San Juan River is substantial compared to other records elsewhere in the region, such a time span may still be too short to correctly identify broader trends or cycles. Besides, additional uncertainties in the modelling of hydrological processes are compounded by the fact that streamflows have been significantly altered by intense human activities (*e.g.*, Tiwari and Chatterjee, 2010). Despite the limitations posed above, we believe that predictive streamflow models are a useful and necessary tool for water resource planning.

5.4. Cryospheric influence on the San Juan River

River streamflow represents a basin's integrated response to climatic processes (Zhang *et al.*, 2009, 2018). In the Arid Andean basins, the greatest water recharge occurs in the highest sector, which coincides with cryospheric development. As a natural system, the cryosphere responds to environmental changes, mostly temperature and precipitation (Hock *et al.*, 2019). Such changes should be considered when analyzing the future hydrological situation in the region. Glacial and periglacial processes and their associated landforms affect the hydrological cycle across different spatial and temporal scales (Jones *et al.*, 2019; Arenson *et al.*, 2022). Seasonal snowmelt combined with surface (glacial) and ground (periglacial) ice melt are the feeding sources for the Cordilleran rivers in the region (Rodríguez *et al.*, 2016; Schaffer *et al.*, 2019).

The San Juan River hydrograph shown in figure 12, reveals, on the one hand, its characteristic behavior over several decades, marked by a pronounced streamflow peak normally occurring between December and January. This peak has a strong component due to snowmelt (Julander and Clayton, 2018) plus an unquantified glacial-periglacial component. On the other hand, the hydrological regime has been altered after the onset of the hydrological drought at around 2010 (Rivera *et al.*, 2021), except for the 2015-2016 and 2016-2017 wet periods. Since 2010, the hydrographs show a fairly stable trend in streamflow values, including a slight streamflow peak towards late summer (February-March). The analysis of snow cover area and percentage of snowy days in the San Juan River basin (https://observatorioandino.com/nieve/), suggests, however, minimal snow accumulation during winter (Ríos *et al.*, 2025; Toum *et al.*, 2025). Such snowpack would explain, to a great extent, streamflows due to melting between the spring and summer periods. At present, the little snow accumulation would generate a stable streamflow without causing any large streamflow peaks. We consider in this work that the faint streamflow peak towards late summer would be due to penetration of the thermal wave into the subsoil and subsequent thawing of the ground ice stored in the active layer. These two causes are enabled by the temporal and spatial decrease of the snow cover, which normally acts as a buffer layer isolating the subsoil from the atmosphere. Besides, we cannot rule out a greater melting of ice contained in the cryoforms due to temperature increases and their influence on streamflows. Future research in this region should therefore analyze the thermal regime and subsoil moisture content to understand its hydrological functioning in depth and its impact on streamflow dynamics.

6. Conclusions

In regions such as the Arid Andes, increases in temperature and decreases in snowfall associated with climate change require comprehensive hydrological studies and streamflow forecasting to evaluate possible

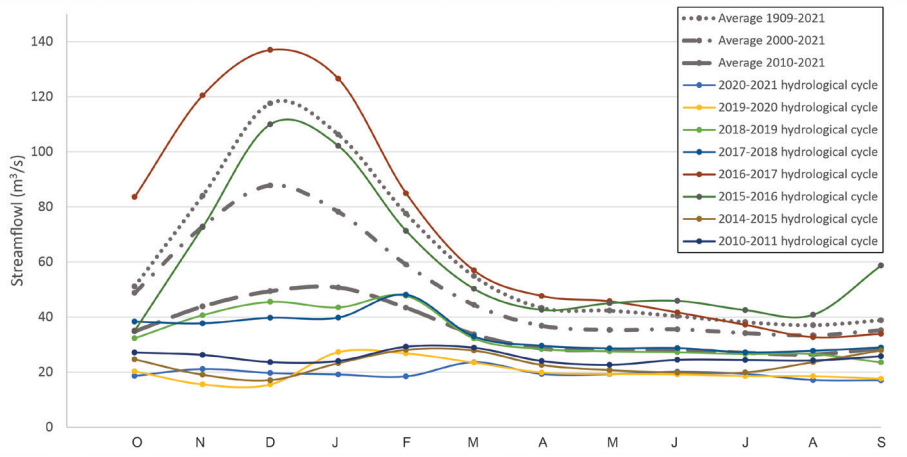

FIG. 12. Monthly streamflow hydrographs of the San Juan River for individual hydrological years (2010-2011 to 2020-2021) and multi-decadal averages (1909-2021, 2000-2021, and 2010-2021). Months from O: October to S: September.

water scarcity scenarios. In the present study, a SARIMA statistical model has been implemented to identify short- and long-term trends, periodicities, and cyclicities in the San Juan River, aimed at forecasting its future behavior over the next 50 years based on a >100-year dataset. Model results identify a general decreasing trend in the river streamflow along with different periodicities in its behavior. The basin's hydrological situation for the next few decades is alarming because annual runoff values will continue to be below those required for human consumption and economic activities. Alternatively, there may be some years or small interspersed periods with abundant available water, although their accuracy needs to be interpreted with caution.

Acknowledgements

We thank Hydraulic Department for collaborating with the delivery of streamflow data for the San Juan River. We are also grateful to the National Council of Scientific and Technical Research (CONICET) and the School of Exact and Natural Sciences of the National University of Cuyo (FCEN-UNCuyo) for their financial support. The authors thank the editor D. Bertin, R. Solorza and one anonymous reviewer for their constructive comments and suggestions, which helped to improve the quality of this manuscript. The data that support the findings of this study are available from the corresponding author upon request.

References

Abraham, E.M.; Rodríguez, M.D.; Rubio, M.C.; Guida-Johnson, B.; Gómez, L.; Rubio, C. 2020. Disentangling the concept of "South American Arid Diagonal". Journal of Arid Environments 175: 104089. https://doi.org/10.1016/j.jaridenv.2019.104089

Arenson, L.U.; Harrington, J.S.; Koenig, C.E.; Wainstein, P.A. 2022. Mountain permafrost hydrology-a practical review following studies from the Andes. Geosciences 12 (2): 48 https://doi.org/10.3390/geosciences12020048

Babel, M.S.; Shinde, V.R.; Sharma, D.; Dang, N.M. 2020. Measuring water security: A vital step for climate change adaptation. Environmental Research 185: https://doi.org/10.1016/j.envres.2020.109400

Biazar, S.M.; Golmohammadi, G.; Nedhunuri, R.R.; Shaghaghi, S.; Mohammadi, K. 2025. Artificial intelligence in hydrology: advancements in soil, water resource management, and sustainable development. Sustainability 17 (5): 2250. https://doi.org/10.3390/su17052250

Box, G.E.P.; Jenkins, G. 1970. Time series analysis, forecasting and control. *In* Time Series Analysis, Forecastingand Control. Holden-Day: 19-553. San Francisco.

Bruniard, E.D. 1982. La diagonal árida argentina: un límite climático real. Revista Geográfica 95: 5-20

Bruniard, E.; Moro, C.O. 1994. Los regímenes fluviales de alimentación sólida en la República Argentina (ensayo de elaboración de un modelo hidroclimático de la vertiente oriental de los Andes). Academia Nacional de Geografía 7: 81 p. Buenos Aires.

Cook, B.I.; Mankin, J.S.; Marvel, K.; Williams, A.P.; Smerdon, J.E.; Anchukaitis, K.J. 2020.Twenty-first century drought projections in the CMIP6 forcing scenarios. Earth's Future 8 (6): e2019EF001461. https://doi.org/10.1029/2019EF001461

Costa, G.; Menezes Filho, F.; Canales, F.; Fava, M.; Brandão, A.;& de Paes, R. 2023. Assessment of Time Series models for Mean Discharge modeling and forecasting in a Sub-basin of the Paranaíba River, Brazil. Hydrology 10 (11): 208. https://doi.org/10.3390/hydrology10110208

Crespo, S.; Aranibar, J.; Gomez,L.; Schwikowski, M.; Bruetsch, S.; Cara, L.; Villalba, R. 2017.Ionic and stable isotope chemistry as indicators of water sources to the Upper Mendoza River basin, Central Andes of Argentina. Hydrological sciences journal 62 (4): 588-605. https://doi.org/10.1080/02626667.2016.1252840

Departamento de Hidráulica. 2022.https://hidraulica.sanjuan.gob.ar/. Accessed in July 2022

Devasthale, A.; Karlsson, K.; Andersson, S.; Engström, E. 2023. Difference between WMO climate normal and climatology: Insights from a satellite-based global cloud and radiation climate data record. Remote Sensing 15 (23): 5598. https://doi.org/10.3390/rs15235598

Dolling, O.; Varas, E. 2002. Artificial neural networks for streamflow prediction. Journal of hydraulic research 40 (5): 547-554. https://doi.org/10.1080/00221680209499899

Fahad, A.; Burls, N.; Strasberg, Z. 2020. How will Southern Hemisphere subtropical anticyclones respond to global warming? Mechanisms and seasonality in CMIP5 and CMIP6 model projections. Climate Dynamics 55 (3-4): 703-718. https://doi.org/10.1007/s00382-020-05290-7

Garreaud, R. 2009.The Andes climate and weather. Advances in Geosciences 22: 3-11. https://doi.org/10.5194/adgeo-22-3-2009

Garreaud, R.; Alvarez-Garreton, C.; Barichivich, J.; Boisier, J.; Christie, D.; Galleguillos, M.; LeQuesne, C.; McPhee, J.; Zambrano-Bigiarini, M. 2017. The 2010-2015 megadrought in central Chile: impacts on regional

hydroclimate and vegetation. Hydrology and earth system sciences 21 (12): 6307-6327. https://doi.org/10.5194/hess-21-6307-2017

Gascoin, S.; Kinnard, C.; Ponce, R.; Lhermitte, S.; MacDonell, S.; Rabatel, A. 2011. Glacier contribution to streamflow in two headwaters of the Huasco River, Dry Andes of Chile. The Cryosphere 5 (4): 1099-1113. https://doi.org/10.5194/tc-5-1099-2011

Ghide, L.; Wei, S.; Ding, Y. 2022. Comparative Study of Wavelet-SARIMA and EMD-SARIMA for Forecasting Daily Temperature Series. International Journal of Analysis and Applications 20: 17-17. https://doi.org/10.28924/2291-8639-20-2022-17

Hock, R.; Rasul, G.; Adler, C.; Cáceres, B.; Gruber, S.; Hirabayashi, Y.; Jackson, M.; Kääb, A.; Kang, S.; Kutuzov, S.; Milner, A.; Molau, U.; Morin, S.; Orlove, B.; Steltzer, H. 2019. High mountain areas. *In* IPCC Special Report on the Ocean and Cryosphere in a Changing Climate (Pörtner, H.; Roberts, D.; Masson-Delmotte, V.; Zhai, P.; Tignor, M.; Poloczanska, E.; Mintenbeck, K.; Alegría, A.; Nicolai, M.; Okem, A.; Petzold, J.; Rama, B.; Weyer, N.; editors). In press.

Hyndman, R.; Khandakar, Y. 2008. Automatic time series forecasting: the forecast package for R. Journal of statistical software 27: 1-22.

Ioannidis, E.E.; Nikolakakou, S.E. 2025. Modeling and Forecasting Stochastic Seasonality: Are Seasonal Autoregressive Integrated Moving Average Models Always the Best Choice?. Journal of Forecasting 45 (1): 316-334. https://doi.org/10.1002/for.70034

Jones, D.; Harrison, S.; Anderson, K.; Whalley, W. 2019. Rock glaciers and mountain hydrology: A review. Earth-Science Reviews 193: 66-90. https://doi.org/10.1016/j.earscirev.2019.04.001

Julander, R.; Clayton, J. 2018. Determining the proportion of streamflow that is generated by cold season processes versus summer rainfall in Utah, USA. Journal of Hydrology: Regional Studies 17: 36-46. https://doi.org/10.1016/j.ejrh.2018.04.005

Kabbilawsh, P.; Kumar, D.S.; Chithra, N.R. 2022. Forecasting long-term monthly precipitation using SARIMA models. Journal of Earth System Science 131 (3): 174. https://doi.org/10.1007/s12040-022-01927-9

Korsic, S.; Notarnicola, C.; Quirno, M.; Cara, L. 2023. Assessing a data-driven approach for monthly runoff prediction in a mountain basin of the Central Andes of Argentina. Environmental Challenges 10: 100680. https://doi.org/10.1016/j.envc.2023.100680

Larance, S.; Wang, J.; Delavar, M.; Fahs, M. 2025. Assessing Water Temperature and Dissolved Oxygen and Their Potential Effects on Aquatic Ecosystem Using a SARIMA Model. Environments 12 (1): 25. https://doi.org/10.3390/environments12010025

Lliboutry, L. 1999. Glaciers of Chile and Argentina. United States Geological Survey professional paper 1386-I-6: 109-206.

Masiokas, M.; Villalba, R.; Luckman, B.; Le Quesne, C.; Aravena, J. 2006. Snowpack variations in the central Andes of Argentina and Chile, 1951-2005: Large-scale atmospheric influences and implications for water resources in the region. Journal of climate 19 (24): 6334-6352.

Massone, H.; Martínez, D.; Vich, A.; Londono, M.; Trombotto, D.; Grondona, S. 2016. Snowmelt contribution to the sustainability of the irrigated Mendoza's Oasis, Argentina: an isotope study. Environmental Earth Sciences 75: 1-11. https://doi.org/10.1175/JCLI3969.1

Minetti, J.; Vargas, W.; Vega, B.; Costa, M. 2007. Las sequías en la pampa húmeda: impacto en la productidad del maíz. Revista brasileira de meteorología 22 (2): 218-232. https://doi.org/10.1590/S0102-77862007000200007

Montecinos, A.; Aceituno, P. 2003. Seasonality of the ENSO-related rainfall variability in central Chile and associated circulation anomalies. Journal of climate 16 (2): 281-296. https://doi.org/10.1175/1520-0442(2003)016<0281:SOTERR>2.0.CO;2

Müller, G.V.; Lovino, M.A. 2023. Variability and Changes in Temperature, Precipitation and Snow in the Desaguadero-Salado-Chadileuvú-Curacó Basin, Argentina. Climate 11 (7). https://doi.org/10.3390/cli11070135

Muthee, S.W.; Kuria, B.T.O.; Mundia, C.N.; Sichangi, A.W.; Kuria, D.N.; Wanjala, J.A.; Kipkemboi, W.; Goebel, M.; Graw, V.; Rienow, A. 2023. Using the SARIMA model to predict the trends of evapotranspiration and runoff in the Muringato river basin, Kenya. Stochastic Environmental Research and Risk Assessment 37 (12): 4707-4718. https://doi.org/10.1007/s00477-023-02534-w

Núñez, J.; Cortés, C.; Yáñez, M. 2023. Explainable Artificial Intelligence in Hydrology: Interpreting Black-Box Snowmelt-Driven Streamflow Predictions in an Arid Andean Basin of North-Central Chile. Water 15 (19): 3369. https://doi.org/10.3390/w15193369

Poblete, A.; Minetti, J. 1989. Los mesoclimas de San Juan. Primera y segunda parte. Informe Técnico 11: 31-32.

Poblete, A.; Hryciw, M. 2017. Origen y variabilidad del recurso hídrico de los principales oasis de la provincia de San Juan. Boletín de Estudios Geográficos 107: 9-20.

Poblete, A.; Minetti, J. 2017. Influye el calentamiento global en la disminución de las nevadas en los Andes Áridos. Revista Universitaria de Geografía 26 (1): 11-29.

Poblete, A.; Castro, M. 2021. Influencia del ENSO en los factores y agentes climáticos que inciden en las precipitaciones níveas de los Andes Áridos. Estudios Socioterritoriales. Revista de Geografía 29: 078-078. https://doi.org/10.37838/unicen/est.29-209

Ríos, L.; Moreiras, S.; Porras, M.; Gómez, M.; D'Ambrosio, D. 2025. Driving factors on wetland water area changes in the arid region of central-western Argentina (32° S) during the last two decades. Andean geology 52 (1): 101-116. http://dx.doi.org/10.5027/andgeoV52n1-3732

Rivera, J.; Penalba, O.; Villalba, R.; Araneo, D. 2017. Spatio-temporal patterns of the 2010-2015 extreme hydrological drought across the Central Andes, Argentina. Water 9 (9): 652. https://doi.org/10.3390/w9090652

Rivera, J.; Otta, S.; Lauro, C.; Zazulie, N. 2021. A decade of hydrological drought in Central-Western Argentina. Frontiers in Water 3. https://doi.org/10.3389/frwa.2021.640544

Rodríguez, M.; Ohlanders, N.; Pellicciotti, F.; Williams, M.; McPhee, J. 2016. Estimating runoff from a glacierized catchment using natural tracers in the semi-arid Andes cordillera. Hydrological processes 30 (20): 3609-3626. https://doi.org/10.1002/hyp.10973

Santos, I.; Herrnegger, M.; Holzmann, H. 2021 Seasonal discharge forecasting for the Upper Danube. Journal of Hydrology: Regional Studies 37. 100905. https://doi.org/10.1016/j.ejrh.2021.100905

Scanlon, B.; Levitt, D.; Reedy, R.; Keese, K.; Sully, M. 2005. Ecological controls on water-cycle response to climate variability in deserts. Proceedings of the National academy of Sciences 102 (17): 6033-6038. https://doi.org/10.1073/pnas.0408571102

Schaffer, N.; MacDonell, S.; Réveillet, M.; Yáñez, E.; Valois, R. 2019 Rock glaciers as a water resource in a changing climate in the semiarid Chilean Andes. Regional Environmental Change 19: 1263-1279. https://doi.org/10.1007/s10113-018-01459-3

Schrott, L. 1991. Global solar radiation, soil temperature and permafrost in the Central Andes, Argentina: a progress report. Permafrost and Periglacial Processes 2 (1): 59-66. https://doi.org/10.1002/ppp.3430020110

Siebert, S.; Burke, J.; Faures, J.; Frenken, K.; Hoogeveen, J.; Döll, P.; Portmann, F. 2010. Groundwater use for irrigation–a global inventory. Hydrology and earth system sciences 14 (10): 1863-1880. https://doi.org/10.5194/hess-14-1863-2010

Subsecretaría de Recursos Hídricos de la Nación. 2009. Estudio Integral de la cuenca del río Desaguadero-Salado-Chadileuvú-Curacó- Colorado. Universidad de Buenos Aires, Facultad de Ingeniería (FIUBA), Departamento de Hidráulica: 208 p. https://recursoshidricos.lapampa.gob.ar/images/Archivos/Publicaciones/DSCHC_Tomo_I_Nov09.pdf

Tapia-Baldis, C.; Trombotto-Liaudat, D. 2020.Permafrost model in coarse-blocky deposits for the Dry Andes, Argentina (28°-33° S). Cuadernos de Investigación Geográfica 46 (1): 33-58. https://doi.org/10.18172/cig.3802

Tapia-Baldis, C.; Trombotto-Liaudat, D.; Ahumada, A. 2019. Ambiente periglacial y regiones geocriológicas en los Andes de San Juan (28º-33ºS). Revista de la Asociación Geológica Argentina 76 (1): 46-63.

Thakur, B.; Kalra, A.; Ahmad, S.; Lamb, K.; Lakshmi, V. 2020. Bringing statistical learning machines together for hydro-climatological predictions-Case study for Sacramento San Joaquin River Basin, California. Journal of Hydrology: Regional Studies 27: 100651. https://doi.org/10.1016/j.ejrh.2019.100651

Tiwari, M.; Chatterjee, C. 2010. Development of an accurate and reliable hourly flood forecasting model using wavelet-bootstrap-ANN (WBANN) hybrid approach. Journal of Hydrology 394 (3-4): 458-470. https://doi.org/10.1016/j.jhydrol.2010.10.001

Toum, E.; Villalba, R.; Masiokas, M. 2025. Snow and glacier contributions to the Mendoza River in the semiarid Central Andes of Argentina. Hydrological Processes 39 (4): e70132. https://doi.org/10.1002/hyp.70132

Valipour, M. 2015. Long-term runoff study using SARIMA and ARIMA models in the United States. Meteorological Application 22 (3): 592-598. https://doi.org/10.1002/met.1491

Viale, M.; Norte, F. 2009. Strong cross-barrier flow under stable conditions producing intense winter orographic precipitation: A case study over the subtropical central Andes. Weather and Forecasting 24 (4): 1009-1031. https://doi.org/10.1175/2009WAF2222168.1

Vich, A.; Lauro, C.; Bizzotto, F.; Vaccarino, E.; Manduca, F. 2016. Recursos hídricos superficiales. Universidad de San Juan: 28 p. San Juan.

Villarroel, C.; Tamburini Beliveau, G.; Forte, A.; Monserrat, O.; Morvillo, M. 2018. DInSAR for a Regional inventory of active rock glaciers in the dry andes mountains of argentina and chile with sentinel-1 data. Remote Sensing 10 (10): 1588. https://doi.org/10.3390/rs10101588

Wang, W.; Van Gelder, P.; Vrijling, J.; Ma, J. 2006 Forecasting daily streamflow using hybrid ANN models. Journal of Hydrology 324 (1-4): 383-399. https://doi.org/10.1016/j.jhydrol.2005.09.032

Wu, M.; Lin, G.; Lin, H. 2014.Improving the forecasts of extreme streamflow by support vector regression with

the data extracted by self-organizing map. Hydrological Processes 28 (2): 386-397. https://doi.org/10.1002/hyp.9584

Zech, J.; Terrizzano, C.; Garcia Morabito, E.; Veit, H.; Zech, R. 2017.Timing and extent of late pleistocene glaciation in the arid Central Andes of Argentina and Chile (22-41 S). Cuadernos de Investigación Geológica 43 (2): 697-718. https://doi.org/10.18172/cig.3235

Zhang, Q.; Xu, C.; Chen, Y; Jiang, J. 2009.Abrupt behaviors of the streamflow of the Pearl River basin and implications for hydrological alterations across the Pearl River Delta, China. Journal of Hydrology 377 (3-4): 274-283. https://doi.org/10.1016/j.jhydrol.2009.08.026

Zhang, X.; Peng, Y.; Zhang, C.; Wang, B. 2015. Are hybrid models integrated with data preprocessing techniques suitable for monthly streamflow forecasting? Some experiment evidences. Journal of Hydrology 530: 137-152. https://doi.org/10.1016/j.jhydrol.2015.09.047

Zhang, Z.; Zhang, Q.; Singh, V.; Shi, P. 2018. River flow modelling: comparison of performance and evaluation of uncertainty using data-driven models and conceptual hydrological model. Stochastic environmental research and risk assessment 32: 2667-2682. https://doi.org/10.1007/s00477-018-1536-y

Manuscript received: March 09, 2025; revised/accepted: January 08, 2026; available online: January 13, 2026.